Nuclear Inst. and Methods in Physics Research, A 1014 (2021) 165663

Contents lists available at ScienceDirect

Nuclear Inst. and Methods in Physics Research, A

journal homepage: www.elsevier.com/locate/nima

An accuracy benchmark of the MIRACLS apparatus: Conventional, single-passage collinear laser spectroscopy inside a MR-ToF device

V. Lagaki [a,b,*], H. Heylen [a], I. Belosevic [c], P. Fischer [b], C. Kanitz [a,d], S. Lechner [a,e], F.M. Maier [a,b], W. Nörtershäuser [f], P. Plattner [a,g], M. Rosenbusch [b,1], S. Sels [a,2], L. Schweikhard [b], M. Vilen [a], F. Wienholtz [a,b,f], R.N. Wolf [b,3], S. Malbrunot-Ettenauer [a]

[a] Experimental Physics Department, CERN, CH-1211 Geneva 23, Switzerland
[b] Institut für Physik, Universität Greifswald, 17487 Greifswald, Germany
[c] TRIUMF, 4004 Wesbrook Mall, Vancouver, BC V6T 2A3, Canada
[d] Department für Physik, Friedrich-Alexander-Universität Erlangen-Nürnberg, 91058 Erlangen, Germany
[e] Technische Universität Wien, Karlsplatz 13, 1040 Wien, Austria
[f] Technische Universität Darmstadt, Institut für Kernphysik, 64289 Darmstadt, Germany
[g] Universität Innsbruck, Innrain 52, 6020 Innsbruck, Austria

ARTICLE INFO

Keywords:
Collinear laser spectroscopy
MR-ToF device
Short-lived radionuclides
MIRACLS

ABSTRACT

Collinear laser spectroscopy (CLS) has been performed in a multi-reflection time-of-flight (MR-ToF) device operated in single-pass mode, i.e., without confining the ions in the ion trap. While our Multi Ion Reflection Apparatus for Collinear Laser Spectroscopy (MIRACLS) aims to increase the CLS sensitivity by storing ions in the MR-ToF device, the present work characterises conventional single-passage CLS as a preparatory step for the upcoming comparison with MIRACLS' multi-pass mode. To this end, the isotope shift in the $3s\,^2S_{1/2} \rightarrow 3p\,^2P_{3/2}$ transition (D2 line) between ions of the magnesium isotopes ^{24}Mg and ^{26}Mg has been measured under varying experimental conditions. Our result agrees with the precise literature value. Associated studies of systematic uncertainties demonstrate a measurement accuracy of better than 20 MHz in this new apparatus. This value will serve as the reference for analogous studies to be performed in the MIRACLS approach in which ions are trapped in the MR-ToF device for thousands of revolutions and probed by the spectroscopy laser during each passage.

1. Introduction

For five decades, atomic-physics techniques have very successfully provided accurate and precise information about nuclear ground state properties of short-lived radionuclides [1–7]. While laser spectroscopy accesses nuclear spins, charge radii and electromagnetic moments, ion traps have become invaluable tools for precision mass measurements.

Within the latter, multi-reflection time-of-flight (MR-ToF) instruments have in recent years emerged in the field of rare isotope science as versatile mass separators and spectrometers [8–16]. In these devices, also called electrostatic ion beam traps [17–19], an ion bunch is reflected between two electrostatic mirrors such that an integrated ion flight path of a few kilometres can be folded into an apparatus with the length of about one metre. Ions of different masses m are consequently separated in mass according to their respective time of flight. Mass resolving powers exceeding $R = m/\Delta m > 10^5$ can be obtained in (tens of) milliseconds [13,20,21].

Given these superb performance characteristics, MR-ToF devices have recently found many applications at modern radioactive ion beam (RIB) facilities. Among others, these include mass measurements of radionuclides very far away from stability with production yields as low as a few ions per second [12,22–24], beam identification for various experimental RIB programmes [25], characterisation and optimisation of RIB production targets for fundamental science as well as medical isotope production [26,27], suppression of contamination in the RIB [28], or mass-tagged ion counting in ion-source laser spectroscopy [29,30].

Our Multi Ion Reflection Apparatus for Collinear Laser Spectroscopy (MIRACLS) developed at ISOLDE/CERN envisions a novel application of MR-ToF devices, namely for highly sensitive laser spectroscopy. To this end, it combines the sensitivity of ion-trap techniques with the

* Corresponding author at: Experimental Physics Department, CERN, CH-1211 Geneva 23, Switzerland.
E-mail address: varvara.lagaki@cern.ch (V. Lagaki).

[1] Current address: Wako Nuclear Science Center (WNSC), Institute of Particle and Nuclear Studies (IPNS), High Energy Accelerator Research Organization (KEK), Japan.

[2] Current address: KU Leuven, Belgium.

[3] Current address: ARC Centre for Engineered Quantum Systems, The University of Sydney, Australia.

https://doi.org/10.1016/j.nima.2021.165663
Received 24 March 2021; Received in revised form 24 June 2021; Accepted 14 July 2021
Available online 17 July 2021

high resolution of collinear laser spectroscopy (CLS) of fast ion beams. In the latter, an ion beam with typical beam energies of $\geq$ 30 keV is collinearly overlapped with a narrow-band, continuous-wave laser beam. When the frequency of the laser corresponds to the energy difference of the studied transition, fluorescence light of laser-excited ions is registered by photon detectors. Hence, the detected photon rate as a function of laser frequency reveals the hyperfine structure which encodes the aforementioned nuclear properties by means of the hyperfine interaction between the atomic nucleus and its surrounding electron cloud.

Although nuclides accessible by CLS exhibit life-times of at least several milliseconds, their effective use in this conventional CLS approach is limited to a few microseconds while the ions pass the laser-ion interaction and optical-detection region. Hence, matching the involved time scales offers the possibility to significantly boost the experimental CLS sensitivity.

Following this vision, MIRACLS aims at confining the fast ion beam inside a MR-ToF device in which the ions are 're-cycled' by continued reflections between the two electrostatic mirrors. Thus, the ion ensemble can be repeatedly probed by the spectroscopy laser during each revolution in contrast to only once for conventional CLS. The MIRACLS approach increases the observation time and, hence, the CLS sensitivity. For instance, in closed two-level systems in which laser-excited ions decay back into their initial state, an ion can in principle be investigated until its radioactive decay. As a result, the MIRACLS approach is expected to yield multiplication factors of 30–700 depending on the half-life, mass and spectroscopic transition of the ions of interest [31].

To demonstrate the strengths of the MIRACLS concept, an MR-ToF apparatus [32,33] has been extended for the implementation of in-trap CLS [34–37]. In particular, the MR-ToF's central drift tube hosts a field-free region for laser-ion interaction and optical detection. Laser access is provided along the axis of the device. While typical ion beam energies in CLS experiments of radionuclides are in the order of several tens of kiloelectron volts, the present setup operates at a beam energy of about 1.5 keV. This will allow proof-of-principle measurements for MIRACLS before the method will be applied in a future 30-keV device.

In the present work, we have as a first step performed conventional, single-passage CLS within this setup in order to benchmark the attainable accuracy for isotope-shift measurements in such an instrument. In particular, we have measured the isotope shift $\delta\nu^{24,26} = \nu_0^{26} - \nu_0^{24}$ in the $3s\,^2S_{1/2} \rightarrow 3p\,^2P_{3/2}$ transition (D2 line) between $^{24}Mg^+$ and $^{26}Mg^+$ ions. We varied the experimental procedures and parameters to expose systematic uncertainties for CLS in this apparatus. Thus, the present study lays the foundations for ongoing work on the MIRACLS technique. It will allow us to disentangle general limitations of this particular CLS implementation at relatively low ion energies from potential influences specifically caused by MR-ToF operation and ion storage.

2. Experimental setup

2.1. MR-ToF apparatus

The experimental apparatus is based on the MR-ToF system described in Ref. [32,33], which was upgraded for the purpose of collinear laser spectroscopy [34–37]. A schematic overview of the setup is shown in Fig. 1a. For the present study, Magnesium (Mg) atoms are ionised inside an electron-impact ion source which closely follows the design in Ref. [38]. Singly-charged ions of stable magnesium isotopes $^{24-26}Mg$ form a continuous beam which is injected into a helium buffer-gas-filled linear Paul trap. The latter consists of two end-cap plates with holes for ion injection and extraction as well as four rods which provide the RF field for radial ion confinement. The rods are longitudinally split into five segments of equal length and establish a DC gradient to drag buffer-gas-cooled ions into a potential minimum next to the downstream end-cap plate.

In order to define the ion loading time and hence the ion number inside the Paul trap, a steering electrode in front of the ion trap is controlled by a fast high voltage (HV) switch which, on demand, guides the ions either into or away from the Paul-trap entrance. The subsequent cooling time, during which no further ions are injected, is typically set to a few milliseconds. Afterwards, the accumulated and cooled ions are released from the trap by lowering the potential of the downstream end-cap plate by another fast HV switch. The extraction pulse is synchronised with respect to the RF phase to ensure identical field conditions during each ion ejection.

The well-defined ion bunches with a typical temporal width of a few hundred nanoseconds are subsequently accelerated for their transfer into the MR-ToF device. In the present work, two different acceleration schemes are utilised, see Fig. 1b. In the first option, which has been used in our previous work [34,35,37], the Paul trap is held at a potential of $U_{pt} \approx 250$ V. After extraction from the Paul trap, the ions are accelerated towards beamline components at $U_{acc} \approx -2080$ V. When the ion bunch reaches the centre of a drift tube, its potential is switched to ground potential (represented by a red, vertical arrow in Fig. 1b). Since this drift tube constitutes in its centre a field-free region, the change in potential is unnoticed by the ions and the pulsed drift tube acts as a 'potential lift'. Hence, the ions exit the drift tube with a kinetic energy of $E_{kin} = e(U_{pt} - U_{acc}) \approx 2330$ eV.

Since HV switching of this pulsed drift tube may lead to some uncertainty in the exact ion beam energy, a second acceleration scheme exclusively based on static potentials is alternatively employed. Considering its common use in CLS, the present work is largely based on this acceleration scheme. It proceeds identically to the previous one, but the acceleration is done towards $U_{acc} = 0$ V such that the drift tube remains on ground potential for the entire measurement cycle. The transfer energy is, hence, solely governed by $E_{kin} = eU_{pt}$. We observe a degraded transfer efficiency for lower ion beam energies, likely due to the increased transverse emittance. Consequently, we permanently raise the Paul trap potential to $U_{pt} \approx 470$ V which is close to its maximum in the present HV configuration.

Independently of the acceleration method, the ion beam subsequently passes an electrostatic quadrupole bender which guides the ions onto the MR-ToF axis. In the present work, all ring electrodes constituting the electrostatic mirrors of the MR-ToF device are left on ground potential. Hence, the ions are not trapped in the ion trap. Surrounded by the electrostatic mirrors, the central drift tube of the MR-Tof device is biased to a potential U_{cdt} such that the ions propagate inside the tube with $E_{kin} = eU_{tot} = e(U_{pt} - U_{acc} - U_{cdt}) \approx 1500$ eV, a kinetic energy typically used during MR-ToF operation. In particular, $U_{cdt} = 830$ V when utilising the lift after the initial acceleration and $U_{cdt} = -1010$ V otherwise.

During setup and ion-beam optimisation, the ions impinge on a retractable ion detector at the end of the setup. At this position, ions of different magnesium isotopes are well resolved in time of flight even without being trapped in the MR-ToF device, see Fig. 2

2.2. Laser setup

The employed laser setup has been discussed in detail in Ref. [37]. In order to study the $3s\,^2S_{1/2} \rightarrow 3p\,^2P_{3/2}$ transition (D2 line) in Mg^+ ions, a laser wavelength of 280 nm ($\lambda^{-1} = 35760.88$ cm^{-1}) is required. In a separate laser laboratory, a diode-pumped solid-state laser pumps a frequency-stabilised dye ring laser which produces a narrow-band, continuous-wave laser beam at 560 nm. The latter is coupled into a high-power optical fibre to transport the laser beam into the about 25-m distant MR-ToF laboratory. There, second-harmonic generation is employed to obtain a laser beam at 280 nm. The output of the frequency doubler is stabilised in power by a proportional–integral (PI) feed-back loop which rotates a $\lambda/2$ plate in front of a polarisation filter in the upstream beam path of the 580 nm laser light and, thus, controls the laser power input into the frequency doubler. After mode

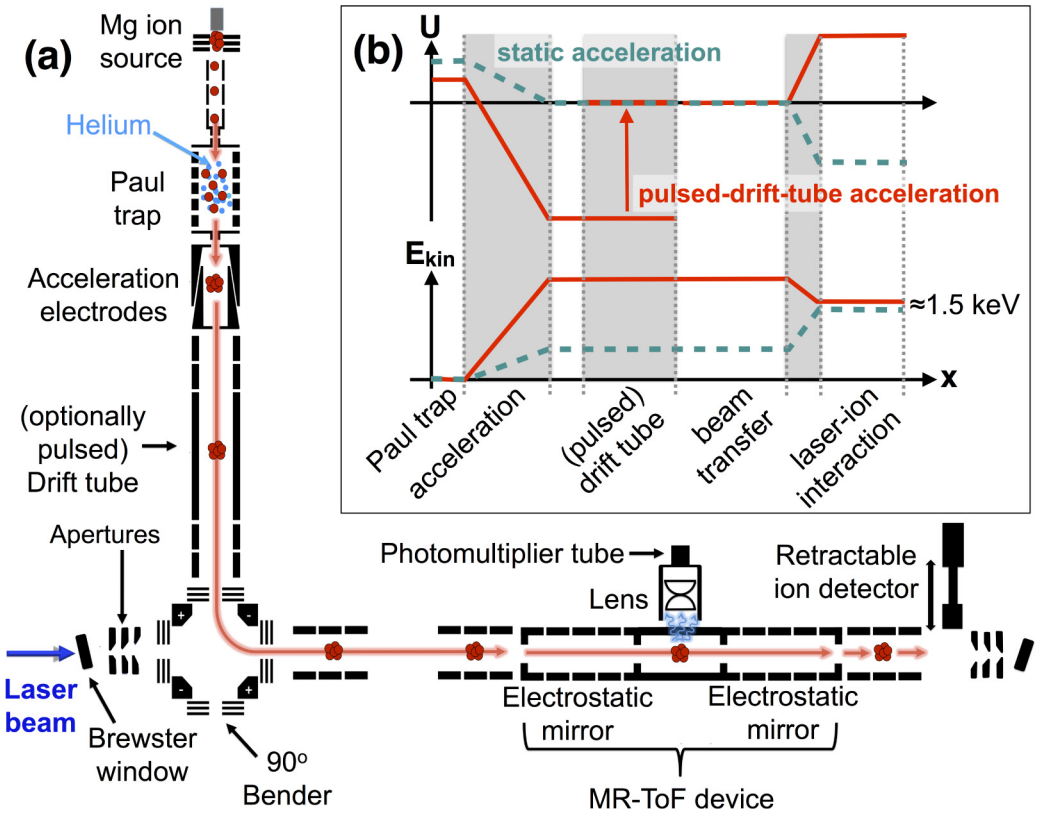

Fig. 1. (a) Schematics of the experimental setup. (b) Sketch of electric potential U and ion beam energy E_{kin} along the path of the Mg^+ ions from the Paul trap to the laser-ion interaction region inside the MR-ToF device. Two different acceleration and ion-transfer schemes are employed. One involves a pulsed drift tube and is represented by the red solid lines. The second one is purely based on static potentials, see turquoise dashed lines. Both result in a final energy of $E_{kin} \approx 1.5$ keV when passing through the laser-ion interaction and optical detection region. See text for details.

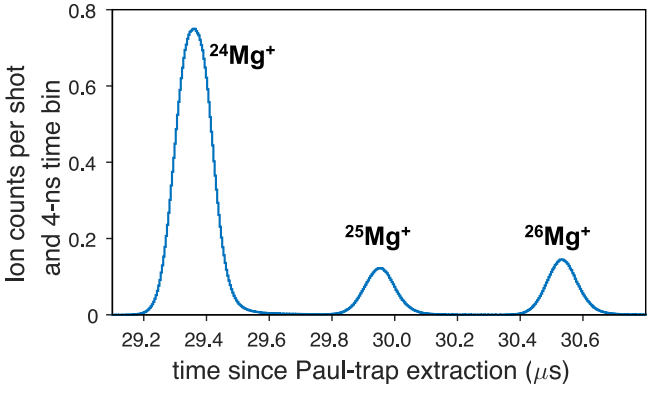

Fig. 2. Time of flight spectrum for ions of stable magnesium isotopes from the Paul trap to the retractable ion detector at the end of the beamline. The peak intensities reflect the natural isotope abundances. The ions are ejected from the Paul trap in the 'fast' extraction mode, accelerated by static potentials, hence without the pulsed drift tube, and pass the MR-ToF device without being trapped. The spectrum is an average of 621'000 ion shots. See text for details.

cleaning to obtain a Gaussian beam profile, the laser beam is sent into the MR-ToF apparatus with a typical power of $\approx$ 0.7 mW and a beam-spot diameter of approximately 2 mm. At its entrance and exit, a quartz window is installed at the Brewster angle, see Fig. 1, to minimise reflections which could potentially lead to undesired laser stray light. The latter is further reduced by aperture sets which are placed in-vacuum next to the entrance and exit windows [36].

The laser frequency is set by locking the dye ring laser to a precision wavemeter (HighFinesse WSU-10) which is regularly calibrated against a temperature-stabilised He-Ne laser. To probe the hyperfine structure of an ion of interest, the laser is scanned across the anticipated frequency range. For each frequency step, photons are recorded for ion bunches released from the Paul trap in multiple measurement cycles.

In this work, two methods are used to scan the laser frequency in the rest frame of the ions. First, the laser frequency in the laboratory reference frame is fixed while the velocity of the ions is changed by altering the potential U_{cdt} of the MR-ToF central drift tube. As ion and laser beams are propagating in the same direction, this results in a Doppler tuning of the laser frequency ν_{ion} observed by the ions according to

$$\nu_{ion} = \nu_{lab} \cdot \frac{1-\beta}{\sqrt{1-\beta^2}}. \quad (1)$$

Here, ν_{lab} represents the laser frequency in the laboratory frame. $\beta = v/c$ is the ion velocity v relative to the speed of light c. This approach is commonly applied in CLS [5].

However, for CLS studies over long isotopic chains or wide hyperfine structures the required difference in energy can be sizable. Within MIRACLS, different ion energies will lead to modified ion trajectories inside the MR-ToF device. This may influence the CLS measurement. For this reason, it is foreseen to operate MIRACLS' MR-ToF device at fixed ion energies and to scan the laser frequency directly in the laboratory frame. Consequently, this scheme, called laser scanning in the following, has also been tested in the present work for conventional, single-passage CLS. In our implementation, the set point of the PID loop which locks the dye laser to the wavemeter is altered in small steps such that the laser cavity follows to the new value. While the laser frequency is being changed all data taking is put on hold until the new set point in the fundamental wavelength has been reached within less than 1.5 MHz. The PID parameters have been optimised for stability as well as fast and reliable changes in frequency, i.e., in our configuration, a frequency step of 10 MHz typically requires a few seconds until completion.

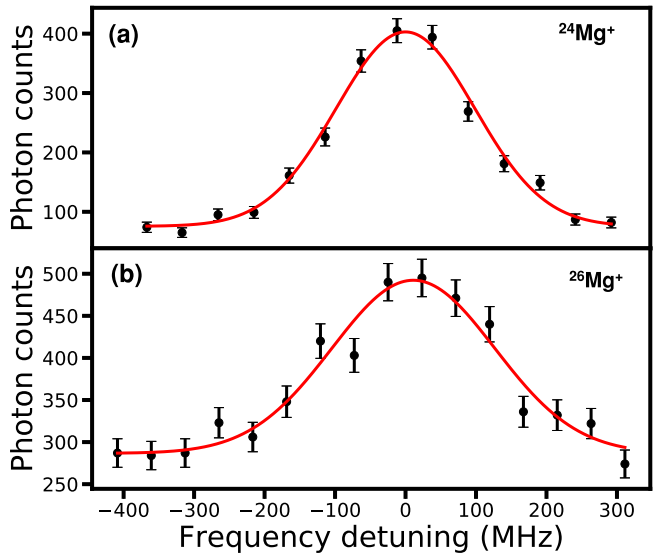

Fig. 3. Measured resonance spectra of the D2 transition in ^{24}Mg$^+$ (a) and ^{26}Mg$^+$ ions (b) performed with laser scanning and a 'fast' Paul-trap extraction scheme as obtained when gating the photon signal on the ions' passage through the optical detection region. The experimental data of photon counts versus laser frequency (in black) is fitted by a Gaussian line shape (in red). The loading time and, hence, the total number of ions in the Paul trap are the same (10 ms) for both runs to ensure identical conditions. The different resonance intensities are a consequence of the natural abundance of the Mg isotopes. The lower abundance of ^{26}Mg is partially compensated by collecting data over, in this case, 4 times more measurement cycles. See text for details.

2.3. Optical detection region and data acquisition

The ion-laser interaction to excite the optical transition takes place in the field-free region of the MR-ToF central drift tube. The latter is constructed from two ring electrodes, approximately 12 cm apart, connected by a cylindrical mesh. This establishes a well-defined electric potential and allows fluorescence light to reach a lens system (adopted from [39]) which directs the photons onto a photomultiplier tube, see Fig. 1a. Around this optical detection region, a blackened shield is mounted [36]. It prevents laser stray light, which does not arise from the ion-beam axis, to be reflected into the lenses and subsequently into the photodetector.

The signal of the photomultiplier tube is passed on to a multichannel scaler which records the number of detected photons versus time since the ions' extraction from the Paul trap. For each laser frequency, the data of multiple measurement cycles, typically a few hundred ion bunches ejected from the Paul trap, are summed. On resonance, the passage of the ion bunch in the optical detection region is visible in the histogram of photon number versus time as a peak of increased photon rate. In our MR-ToF setup, which has initially been designed for other purposes than CLS, laser stray light scattered from beamline components largely dominates the photon background. During the present measurements, it typically accounts for a background rate of $\approx$ 150 kHz when a laser beam of $\approx$ 0.7 mW in power and $\approx$ 2 mm in diameter is used. To suppress the background counts, the signal is gated in the analysis on the ion passage.

3. Measurement procedure and analysis

Typical resonances of ^{24}Mg$^+$ and ^{26}Mg$^+$ ions are shown in Fig. 3. Since both Mg isotopes are nuclides with nuclear spin $I = 0$, there is no hyperfine splitting and, thus, only a single peak is present in the resonance spectra. For a resonance scan, each laser frequency ν_{lab} is converted to the ions' rest frame frequency, ν_{ion}, according to Eq. (1). For an ion with mass m accelerated by an overall acceleration potential U_{tot} this becomes

$$\nu_{\mathrm{ion}} = \nu_{\mathrm{lab}} \frac{eU_{\mathrm{tot}} + mc^2}{mc^2} \left(1 - \sqrt{1 - \frac{m^2c^4}{(eU_{\mathrm{tot}} + mc^2)^2}} \right), \tag{2}$$

where e is the elementary charge. In the calculation of U_{tot}, we assume U_{pt}, the starting potential from which the ions are released from the Paul trap, to be the mean value of the DC potentials applied to two segments which form the bottom of the well in the Paul trap, see later discussion in Section 4.1.1. All relevant electrical potentials are measured on a regular basis with high-precision voltage dividers (Julie Research KV10). This includes measurements of the individual voltage steps when scanning the potential of the MR-ToF central drift tube during Doppler tuning.

Due to the relatively low beam energy of $E_{\mathrm{kin}} \approx 1.5$ keV, the observed full width at half maximum (FWHM) of the experimental resonances is $\approx$ 250 MHz, i.e., much larger than the natural line width of 42 MHz of the D2 transition. Hence, the line width is dominated by Doppler broadening which results in a Gaussian line shape. Assuming that the line width is entirely governed by the ions' energy distribution, the FWHM in Fig. 3a corresponds to an energy spread of $\approx$ 1.8 eV at the given ion energy. All resonance spectra are fitted by a Gaussian line profile utilising a χ^2-minimisation procedure in the SATLAS analysis package [40] to obtain the respective centroid frequency ν_0.

Each individual isotope-shift measurement $\delta\nu^{24,26}$ between ^{24}Mg$^+$ and ^{26}Mg$^+$ ions is initiated by the calibration of the wavemeter. Subsequently, CLS is performed by recording two ^{24}Mg$^+$ resonance spectra interleaved with one of ^{26}Mg$^+$ ions under identical measurement conditions. Because of its lower natural abundance, measurements with ^{26}Mg$^+$ ions last significantly longer than for ^{24}Mg$^+$ ions to obtain resonance spectra of comparable quality. The two independent ^{24}Mg measurements also serve as a measure of potential drifts in the system during the longer data taking of ^{26}Mg$^+$ ions. For this purpose, the weighted average of the ^{24}Mg measurements, $\bar{\nu}_0^{24}$, and the associated Birge ratio R_B [41][4] are evaluated. Following the procedures adopted by the Particle Data Group [42], we inflate the uncertainty on $\bar{\nu}_0^{24}$ by the Birge ratio in case the latter is larger than one. Finally, the isotope shift is calculated following $\delta\nu^{24,26} = \nu_0^{26} - \nu_0^{24}$.

With the aim to expose potential systematic errors in our apparatus, we have performed measurements of this isotope shift under various experimental conditions. These include different measurement schemes which could impact the ions' beam energy, i.e., (1.1) different ion extraction schemes from the Paul trap as well as (1.2) the two methods in ion acceleration as explained in Section 2.1. For the former, we use two different field gradients in the Paul trap resulting in a 'slow' or a 'fast' release from the ion trap, respectively. Moreover, (2) the Paul-trap loading time and, hence, ion numbers are varied to investigate space-charge effects in the ion trap. Finally, (3) the laser frequency as observed by the moving ions is changed via either laser scanning or Doppler tuning. Table 1 summarises all isotope-shift measurements in this work according to their respective experimental configurations.

In each measurement setting, $\delta\nu^{24,26}$ is determined multiple times and a weighted average is constructed. The uncertainty of the latter is inflated following the previously explained procedure in case of a Birge ratio $R_B > 1$ which indicates that the variations within the individual measurements exceed the statistically expected fluctuations. Fig. 4a and b provide examples for individual isotope-shift measurements in selected measurement configurations, discussed in detail next.

[4] For a set of n measurements x_i with an uncertainty σ_i, the Birge ratio is defined as

$$R_B = \sqrt{\chi^2/(n-1)} = \sqrt{\frac{1}{1-n}\sum_{i=1}^{n}\frac{(x_i - \bar{x})^2}{\sigma_i^2}}, \tag{3}$$

where $\bar{x}$ is the weighted average over all individual measurements x_i.

Table 1
Overview of all isotope-shift measurements in this work indicating the used ion-acceleration scheme (Accel.), the Paul-trap extraction mode, the Paul-trap loading time, as well as the employed method of frequency scanning, i.e., laser scanning or Doppler tuning. The number of individual isotope-shift measurements for each setting is listed in the last column.

#	Accel.	Paul-trap extraction	Loading time (ms)	Scanning mode	# of IS
1	static	fast	5	laser	5
2	static	fast	10	laser	5
3	static	slow	20	laser	5
4	static	fast	20	laser	1
5	static	slow	10	Doppler	3
6	static	slow	20	Doppler	2
7	lift	fast	≤1	laser	2

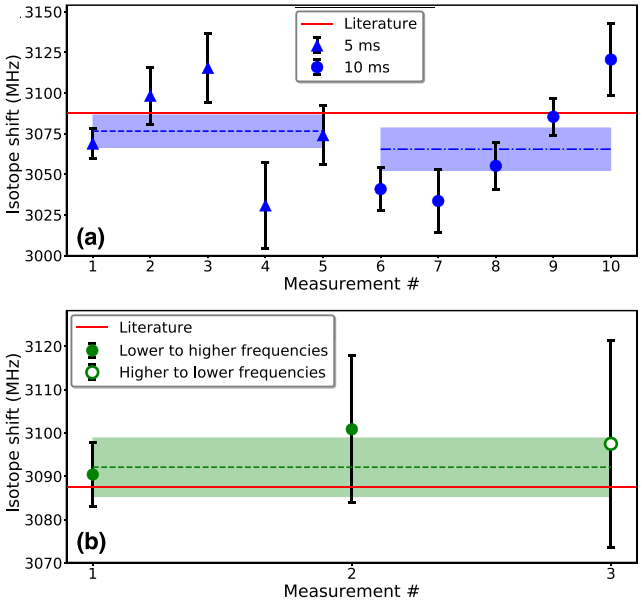

Fig. 4. Examples of individual isotopes-shift measurements $\delta\nu^{24,26}$. (a) Results for different Paul-trap loading times for measurements performed with laser scanning and a 'fast' ion extraction. (b) $\delta\nu^{24,26}$ results for Doppler tuning from either lower to higher frequency or vice versa. A 'slow' ion extraction and a 10-ms loading time is employed. The respective weighted average of the individual measurements is indicated as a dashed line and its uncertainty is represented by the shaded area. For comparison, the precise literature value is shown in red. See text for details.

4. Results and discussion

As stated above, the aim of the present measurement campaign is to determine the isotope shift $\delta\nu^{24,26}$ between $^{24}Mg^+$ and $^{26}Mg^+$ ions in the D2 transition in order to isolate systematic uncertainties of the new apparatus arising from everything except for the MR-ToF operation itself. The results of the different measurement schemes as introduced above are compared to each other in Fig. 5. As a final accuracy benchmark, the present isotope-shift value is compared to its much more precise determination of $\delta\nu^{24,26} = 3087.560(87)$ MHz, measured using laser- and sympathetically-cooled Mg^+ ions stored in a Paul trap [43]. In the following, we discuss the results as well as all systematic uncertainties identified in this work.

4.1. Ion beam energy

In CLS, the dominating systematic uncertainty is normally related to an incomplete knowledge of the ion beam energy E_{kin}. For conventional CLS with $E_{kin} \geq 30$ keV, this is due to the uncertainty of the high-precision voltage dividers which are used to measure the

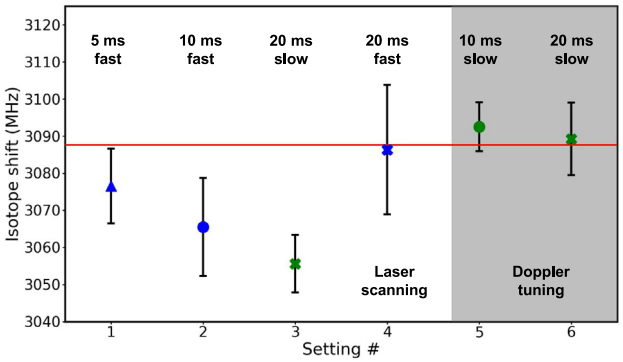

Fig. 5. Results of the systematic investigations in the isotopes shift $\delta\nu^{24,26}$ within the MIRACLS apparatus with conventional, single-passage CLS. For all displayed measurements, the ions are accelerated by static potentials. Each data point corresponds to the weighted average of several individual measurements within a given measurement settings. The latter are characterised by their frequency-scanning method (laser scanning or Doppler tuning), Paul-trap extraction scheme ('slow' or 'fast'), and the Paul-trap loading time. See text for details.

acceleration potentials, e.g. the floating potential of the ion source or of a Paul trap acting as an ion cooler and buncher.

In our work, the largest systematic uncertainty is also found in E_{kin}. However, at the smaller electrostatic potentials and ion energies in our setup, the larger contribution arises due to uncertainties in the ions' starting potential within the Paul trap itself. Moreover, the actual time dependence of the HV-switching process for the pulsed drift tube can result in an ion beam energy which differs from the expectation of the idealised lift operation. The two effects are discussed in the following subsections.

4.1.1. Starting potential U_{pt} in the Paul trap

The voltage applied to the DC electrodes at the bottom of the Paul-trap's potential well is not necessarily the same as the potential to which the ions are exposed. Moreover, the process of ion extraction from the ion trap may further affect the ions' kinetic energy E_{kin}. Both factors are of concern for conventional CLS of bunched beams in general. However, these effects are commonly surpassed in magnitude by the uncertainties in the voltage-divider ratio when working with $E_{kin} \geq 30$ keV.

In order to estimate the ions' starting potential in our Paul trap, the electric potential within a 3D model of the ion trap is determined by solving the Laplace equation in a finite-difference method. The results of the calculations are shown in Fig. 6 for ion trapping as well as for two potential configurations by which the ions are released from the trap. We refer to the latter as 'slow' and 'fast' ion extraction, respectively, reflecting the smaller and larger potential gradient during initial ion acceleration. The three configurations differ in their respective potential applied to the end cap, which is 485 V for trapping, 447 V for 'slow' and 407 V for 'fast' extraction.

In the ion trapping mode, the minimum of the potential well is determined which also defines the mean ion position at the time of the extraction. The potential's value at this minimum would represent the initial ion potential U_{pt} if the ions were directly released from this minimum. In practice, the HV switching of the end cap will influence the ions' starting potential U_{pt}. In case of an infinitely fast HV switching, for instance, the ions would instantaneously 'drop' to the potential evaluated at the same axial position but in the configuration of ion extraction. The corresponding values are indicated in Fig. 6 by coloured arrows for 'slow' and 'fast' ion extraction, respectively. The correct potential value U_{pt} should be somewhere in-between the extreme scenarios of infinitely fast HV switching and the minimum of the potential well during ion trapping.

Since the exact starting potential in the Paul trap U_{pt} with realistic HV switches is not known, we assume U_{pt} in the analysis to be the mean

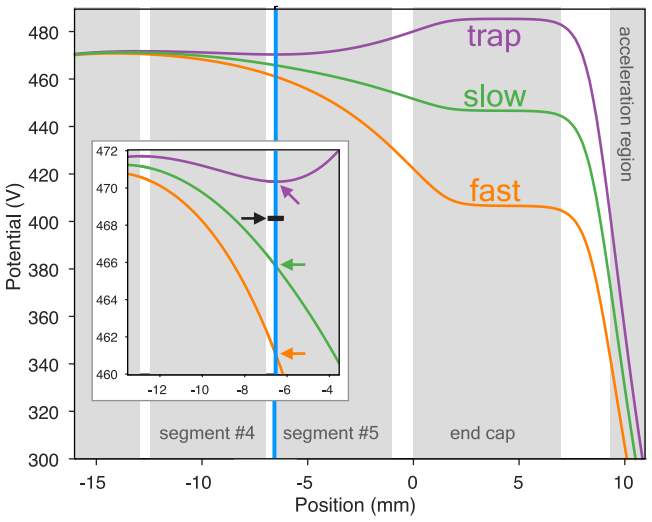

Fig. 6. Electrostatic potential along the axis of the Paul trap during ion trapping as well as for the 'slow' and 'fast' ion extraction. The inset provides a closer look on the trapping region. The vertical blue line indicates the location of the potential minimum during trapping. The coloured arrows point to the potential's value at this location for all three configurations. The black arrow indicates the mean value of the voltages applied to the electrodes of segment 4 and 5. The grey shaded areas are the extensions of the electrodes. See text for details.

of the DC potentials applied to the two electrodes at the bottom of the Paul-trap well (Segment 4 and 5 in Fig. 6), as mentioned already in Section 2.1. This U_{pt} potential is very close to the mid-value between the potentials of trapping and 'slow' extraction, see Fig. 6.

Additionally, to constrain the possible impact of the ions' starting potential on the isotope shift, we determine the potential at the trap minimum for trapping as well as extraction (see again coloured arrows in the inset Fig. 6). These values are then used in the calculation of the ion-beam energy and the respective isotope shift $\nu_0^{24,26}$ is determined. Considering these values, we take the maximal difference to the result with the previously assumed U_{pt} as the systematic uncertainty in $\nu_0^{24,26}$. This corresponds to ± 12 MHz in 'slow' and $+12/-40$ MHz in 'fast' extraction, respectively. Note that this systematic uncertainty is not included in Fig. 5 since it correlates the individual uncertainties, i.e., it shifts all values in the same direction and, within each group of identical extraction schemes, also by the same amount.

Experimentally, no statistically significant difference between the results of 'slow' and 'fast' extraction is observed, see Fig. 5. Since the uncertainties of isotope-shift measurements performed with 'slow' ion extraction are much smaller, both in statistics as well as systematics, their weight dominates the entire data set. Because of the reasonable agreement in the results of 'slow' and 'fast' extraction, we consequently adopt a systematic uncertainty of ± 12 MHz for incomplete knowledge of the ions' starting potential in the present work.

4.1.2. Pulsed drift tube

Pulsed drift tubes are commonly employed in ion-trap installations as they provide an elegant solution to define ion energies independently of the electrostatic potentials of vacuum chambers and beamlines. In CLS, however, these potential lifts are generally avoided since accurate knowledge of the ion-beam energy is indispensable. The operation of the pulsed drift tube as part of the ion acceleration can affect the ion beam energy in an unexpected way such that E_{kin} differs from the expectation in an idealised lift. Indeed, when assuming the nominal acceleration voltages related to the pulsed drift tube in this work, see Section 2.1, we obtain an isotope shift $\nu_0^{24,26}$ which is about 200 MHz larger than the literature value.

Because of the non-vanishing capacitance of the pulsed drift tube and practical limitations of electric circuits, the HV switching of the drift tube cannot be performed in the form of an ideal step function. As a consequence, the ions may exit the lift before its final potential is reached. In our case, the HV switch is operated in a slightly over-damped mode, i.e., without major oscillations in voltage at the beginning of the HV switching. This will result in a lower ion energy compared to the estimate based on the nominal switch voltages. Assuming both isotopes are affected the same, a shift of 200 MHz in the isotope shift would correspond to $\approx$ 40 V in the acceleration potential. This is about 2% of the HV switched at the pulsed drift tube. Measurements of the HV switching suggest that this value reflects the right order of magnitude. We hence conclude that the use of a pulsed drift tube for accurate CLS requires detailed knowledge about the process of the respective HV switching or a sufficiently-long lift electrode. Measurements utilising the pulsed drift tube will thus not be considered further in the present work.

4.2. Paul-trap loading time and space-charge effects

Due to their Coulomb force interactions, the number of ions stored in the Paul trap has an influence on the properties of the ion ensemble. For CLS of bunched beams, these so-called space-charge effects may cause sizable shifts in the resonance centroids. To study their importance in our apparatus, different loading times of the Paul trap and, hence, numbers of stored ions are explored.[5]

Compared to other Paul traps exploited for CLS, ours is relatively small. For instance, ISOLDE's cooler and buncher ISCOOL [46,47] is operated for CLS applications with a flatter axial potential, among others, as three DC segments of each 9 mm in length are biased to the same voltage. Consequently, up to 10^6 ions can be simultaneously prepared in ISCOOL without affecting the CLS resonance spectrum.

In our trap, however, we notice space-charge effects already at much lower ion numbers. For example, Fig. 7b shows the measured centroid frequency of ^{24}Mg, ν_0^{24}, for different Paul-trap loading times. The centroid clearly increases with increasing loading time. This effect is much larger than frequency drifts in the system over time, as illustrated by three measurements at 5 ms in Fig. 7b which are taken at the beginning, middle and end of this measurements series.

Data for loading times of $\leq$ 1 ms, see also Fig. 7a, may indicate an operation below the trap's limit in ion number at which the CLS performance becomes notably influenced by space-charge effects. However, the experimental uncertainties are too large to fully confirm the independence of ν_0 from the ion number. A loading time of 1 ms corresponds to $\approx$ 900 ^{24}Mg$^+$ ions per ion bunch at the end of the beamline when the ion number registered by the ion detector at low rates is scaled by the loading time.

In Fig. 4a, the implications of space-charge effects on the isotope shift are illustrated. While all other measurement settings remain identical, individual isotope shifts as well as their weighted averages are shown for the Paul-trap loading times of 5 ms and 10 ms. Within uncertainties, the isotope shifts for both loading times agree with each other. Hence, the shift in ν_0 cancels in the isotope shift $\delta\nu^{24,26}$ in our work. This can be explained by the fact that ions of all Mg isotopes are stored simultaneously in the Paul trap. Thus, when the same loading time is used for measurements of ^{24}Mg and ^{26}Mg, both isotopes appear to be similarly affected by the space charge of the single cloud of mixed isotopes.

[5] We note that the loading time is an incomplete parameterisation of the ion number. For instance, the ion-source current may change over a period of several measurement days resulting in different ion numbers despite the same loading time. At this time, we do not have the means to reliably determine the number of ions in an ion bunch. Our best estimate relies on single-ion counting at low intensities which is then scaled to longer loading times when pile-up in the ion detection occurs. This approach assumes a strict linearity between ion number and loading time. Although previous work suggests that such a linearity holds at least for the presently used loading times [44,45], it is not established with certainty in this work. Hence, we prefer to state the loading time instead of an estimated ion number, despite the former's aforementioned limitations.

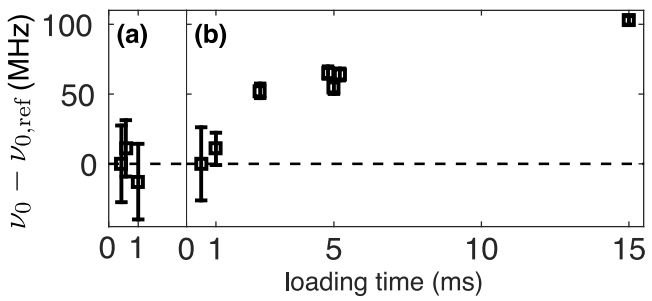

Fig. 7. Resonance centroids ν_0 of $^{24}Mg^+$ ions for different Paul-trap loading times compared to a reference value $\nu_{0,\mathrm{ref}}$ corresponding to a measurement with a loading time of 0.5 ms. (a) and (b) represent two independent measurements sets. See text for details.

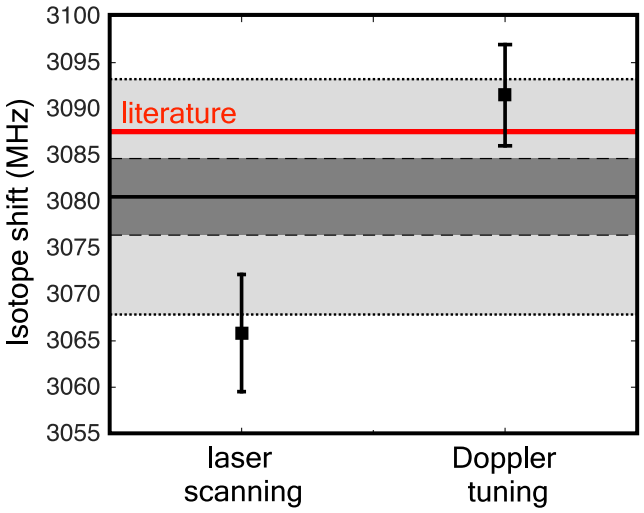

Fig. 8. Isotope shift $\nu_0^{24,26}$ obtained by laser scanning and Doppler tuning. The weighted average of the two is indicated by the black line. The dark grey band represents the statistical uncertainty while the light grey band is the inflated uncertainty reflecting a systematic uncertainty on the isotope shift between these two scanning methods. Note that the systematic error due to the ions' starting potential is not included in the given data. See text for details.

4.3. Doppler tuning versus laser scanning

As discussed earlier, Doppler tuning is realised for a subset of the isotope-shift measurements by scanning the voltage applied to the MR-ToF's central drift tube. Fig. 4b presents the results of one Doppler-tuning data set. By introducing a sufficiently long waiting time in the measurement cycle, it is ensured that each voltage step is completed prior to data taking. To investigate potential remaining effects, the direction of the voltage scanning has been reversed. As shown in Fig. 4b, the respective results agree within their statistical uncertainties.

In addition to Doppler tuning, data sets are recorded with scanning the laser frequency in the laboratory frame. As visible in Fig. 5, a discrepancy between $\nu_0^{24,26}$ obtained from Doppler tuning and from laser scanning is observed. Since there is no evidence of systematic errors due to the other experimentally tested configurations, we combine all results from each frequency-scanning method. From a statistical perspective, each of these sets itself represents a fairly consistent data set. However, as shown by Fig. 8, the weighted averages in $\nu_0^{24,26}$ of laser scanning and of Doppler tuning are not consistent with each other. Note that the plotted values for $\nu_0^{24,26}$ do not consider the systematic uncertainty due to the ions' starting potential, see Section 4.1.1. This accounts for 12 MHz in $\nu_0^{24,26}$ when considering the 'slow' extraction scheme, but also correlates the two results. If this systematic effect shifts one of them towards a higher value of $\nu_0^{24,26}$, the second result will follow in the same direction, too. Hence, although voltage scanning is favoured, the comparison of the data to the accurate literature value does not unambiguously resolve whether a method of frequency scanning is fully robust against systematic errors. Consequently, we proceed by following the previously introduced prescription and inflate the uncertainty on the weighted average of the two data sets with the Birge ratio R_B. Considering that systematic and statistical error should add in quadrature to this inflated uncertainty, we assign a systematic uncertainty of $\sigma_{\mathrm{sys,FS}} = \sigma_{\mathrm{stat}}\sqrt{R_B^2 - 1} = 12\,\mathrm{MHz}$ due to the frequency-scanning methods in this work.

While Doppler tuning is the most commonly applied method in CLS, laser scanning is, for instance, employed by the CRIS collaboration at an accuracy of better than 1 MHz for isotope shifts, see Ref. [48,49] for measurements in a similar mass range. The implementation of laser scanning in the present work proceeds similarly but differs in three technical aspects. Firstly, our wavemeter operates at a lower accuracy compared to the device employed by the CRIS collaboration. Secondly, instead of a He-Ne laser in our work, the wavemeter at CRIS is more accurately calibrated by a diode laser which is locked to a transition in rubidium or potassium atoms. Finally, the beams of diode laser and spectroscopy laser are coupled at CRIS into a Fabry–Perot interferometer for laser frequency monitoring and calibration [48].

Recently, the performance of various precision wavemeters has been investigated in great detail [50,51]. These studies indicate that measurements by a wavemeter similar to ours can show inaccuracies of up to ±5 MHz which follow a non-linear, periodic pattern over a scanning range of ≈ 2 GHz [50].

In our work, the wavemeter is used to lock the frequency of the fundamental wavelength to 560 nm. As a consequence of the frequency doubling to 280 nm, the effect of the wavemeter's relative inaccuracy is thus amplified by a factor of two. The resonances of $^{24}Mg^+$ and $^{26}Mg^+$ ions are approximately 12 GHz apart in their laboratory-frame frequencies. Hence, if the resonances of $^{24}Mg^+$ and $^{26}Mg^+$ ions happen to be close to opposite extremes in the wavemeter's deviation, a shift of up to 20 MHz could occur in either direction in the isotope shift $\nu_0^{24,26}$. For this reason, the systematic uncertainty of 12 MHz assigned above to our experiment's frequency scanning may potentially be caused entirely by the wavemeter.

4.4. Final result for $\nu_0^{24,26}$ and measurement accuracy of the apparatus

We obtain $\nu_0^{24,26} = (3081 \pm 4 \pm 17)$ MHz for the isotope shift in the D2 transition between $^{24}Mg^+$ and $^{26}Mg^+$ ions. Here, the uncertainty is separated into statistical and systematic contributions. The latter consists of uncertainties due to ion's starting potential in the Paul trap (12 MHz, see Section 4.1.1) as well as the frequency-scanning methods (12 MHz, see Section 4.3). Both systematic uncertainties are added in quadrature. The measured value $\nu_0^{24,26}$ is in agreement with the more precise literature value [43]. This demonstrates an accuracy of the present setup for conventional CLS at a level better than 20 MHz.

5. Conclusion and outlook

As part of the developments towards the Multi Reflection Ion Apparatus for Collinear Laser Spectroscopy (MIRACLS), we have performed conventional, single-passage collinear laser spectroscopy (CLS) in an MR-ToF device. In particular, the isotope shift of the well-known $3s\,^2S_{1/2} \rightarrow 3p\,^2P_{3/2}$ transition between $^{26}Mg^+$ and $^{24}Mg^+$ ions has been determined.

The measured isotope shift is in agreement with the more precise literature value. We have performed these measurements under varying experimental conditions to evaluate systematic uncertainties in our new apparatus.

One identified systematic uncertainty is due to the ions' starting potential in the Paul trap which influences the final ion beam energy. We

estimate this uncertainty based on calculations of the axial potentials in the Paul trap. To reduce this uncertainty further, 'slower' ion extraction schemes from the Paul trap will be employed in future work.

Reflecting a second systematic uncertainty, a discrepancy between the results from Doppler tuning and laser scanning is observed. Its size is consistent with inaccuracies of the wavemeter. Ongoing CLS work performed on ions trapped in the MR-ToF device relies on laser scanning only. For this method, we assign a systematic uncertainty of 20 MHz in the isotope shift caused by the wavemeter, see Section 4.3. Ultimately, our implementation of laser scanning needs to be upgraded, as it has been shown to yield accurate isotope-shift results by other groups [48].

The present work also demonstrates that the use of a pulsed drift tube as a 'potential lift' in the ion acceleration severely affects a CLS measurement. In particular, a sizable difference in the isotope shift to the literature value is observed. This is associated with the high-voltage (HV) switching of the pulsed drift tube which inflates the ion beam energy in a non-trivial way. Although not relevant for the present result, the HV switching of electrode(s) is necessary for MR-ToF operation at MIRACLS, i.e., during ion capture into the ion trap. Ongoing work is hence dedicated to fully characterise the HV-switching process.

Overall, the present work establishes that a measurement accuracy of about 20 MHz in isotope shifts is feasible in this new apparatus for conventional, single-passage CLS at an ion beam energy of ≈ 1.5 keV. In a next step, we are performing CLS studies in the MIRACLS approach, i.e., by trapping the ions in the MR-ToF device. The comparison to the present results will allow us to quantify the influence of the MR-ToF operation on the CLS performance, especially in terms of the measurement accuracy as well as the sensitivity advantage of the multi-reflection scheme with respect to the present single-passage measurements.

Declaration of competing interest

The authors declare that they have no known competing financial interests or personal relationships that could have appeared to influence the work reported in this paper.

Acknowledgements

The research leading to these results has received funding from the European Research Council (ERC) under the European Union's Horizon 2020 research and innovation programme under grant agreement No. 679038. L.S. and P.F. acknowledge support by the German Ministry for Education and Research (BMBF, 05P18HGCIA). Part of the work of F.M.M. has been sponsored by the Wolfgang Gentner Programme of the German Federal Ministry of Education and Research (grant no. 05E18CHA). We are grateful for support from CERN, the ISOLDE Collaboration, and the Max–Planck-Institut für Kernphysik (MPI K) in Heidelberg. We would like to thank S. Sailer, L. E. Fischer, L. M. Bartels, and F. Hummer for their earlier contributions to MIRACLS.

References

[1] J. Bonn, G. Huber, H. Kluge, U. Köpf, L. Kugler, E.-W. Otten, Optical pumping of neutron deficient 187Hg, Phys. Lett. B 36 (1) (1971) 41–43.

[2] G. Bollen, P. Dabkiewicz, P. Egelhof, T. Hilberath, H. Kalinowsky, F. Kern, H. Schnatz, L. Schweikhard, H. Stolzenberg, R.B. Moore, H.J. Kluge, G.M. Temmer, G. Ulm, First absolute mass measurements of short-lived isotopes, Hyperfine Interact. 38 (12) (1987) 793–802.

[3] E.W. Otten, Nuclear Radii and Moments of Unstable Isotopes, Springer US, Boston, MA, 1989, pp. 517–638.

[4] H.-J. Kluge, Precision measurements of masses of radioactive atoms using ISOLDE and ion traps, Phys. Scr. T22 (1) (1988) 85–89.

[5] K. Blaum, J. Dilling, W. Nörtershäuser, Precision atomic physics techniques for nuclear physics with radioactive beams, Phys. Scr. 2013 (T152) (2013) 014017.

[6] R. Neugart, J. Billowes, M.L. Bissell, K. Blaum, B. Cheal, K.T. Flanagan, G. Neyens, W. Nörtershäuser, D.T. Yordanov, Collinear laser spectroscopy at ISOLDE: new methods and highlights, J. Phys. G: Nucl. Part. Phys. 44 (apr) (2017) 064002.

[7] J. Dilling, K. Blaum, M. Brodeur, S. Eliseev, Penning-trap mass measurements in atomic and nuclear physics, Annu. Rev. Nucl. Part. Sci. 68 (1) (2018) 45–74.

[8] W.R. Plaß, T. Dickel, U. Czok, H. Geissel, M. Petrick, K. Reinheimer, C. Scheidenberger, M. I.Yavor, Isobar separation by time-of-flight mass spectrometry for low-energy radioactive ion beam facilities, Nucl. Instrum. Methods Phys. Res. B 266 (19–20) (2008) 4560–4564.

[9] A. Piechaczek, V. Shchepunov, H.K. Carter, J.C. Batchelder, E.F. Zganjar, S.N. Liddick, H. Wollnik, Y. Hu, B.O. Griffith, Development of a high resolution isobar separator for study of exotic decays, Nucl. Instrum. Methods Phys. Res. B 266 (19) (2008) 4510–4514.

[10] P. Schury, K. Okada, S. Shchepunov, T. Sonoda, A. Takamine, M. Wada, H. Wollnik, Y. Yamazaki, Multi-reflection time-of-flight mass spectrograph for short-lived radioactive ions, Eur. Phys. J. A 42 (3) (2009) 343.

[11] R. Wolf, F. Wienholtz, D. Atanasov, D. Beck, K. Blaum, C. Borgmann, F. Herfurth, M. Kowalska, S. Kreim, Y.A. Litvinov, D. Lunney, V. Manea, D. Neidherr, M. Rosenbusch, L. Schweikhard, J. Stanja, K. Zuber, Isoltrap's multi-reflection time-of-flight mass separator/spectrometer, in: 100 years of Mass Spectrometry, Int. J. Mass Spectrom. 349–350 (2013) 123–133.

[12] F. Wienholtz, D. Beck, K. Blaum, C. Borgmann, M. Breitenfeldt, R.B. Cakirli, S. George, F. Herfurth, J.D. Holt, M. Kowalska, S. Kreim, D. Lunney, V. Manea, J. Menéndez, D. Neidherr, M. Rosenbusch, L. Schweikhard, A. Schwenk, J. Simonis, J. Stanja, R.N. Wolf, K. Zuber, Masses of exotic calcium isotopes pin down nuclear forces, Nature 498 (7454) (2013) 346–349.

[13] T. Dickel, W. Plaß, A. Becker, U. Czok, H. Geissel, E. Haettner, C. Jesch, W. Kinsel, M. Petrick, C. Scheidenberger, A. Simon, M. Yavor, A high-performance multiple-reflection time-of-flight mass spectrometer and isobar separator for the research with exotic nuclei, Nucl. Instrum. Methods Phys. Res. A 777 (2015) 172–188.

[14] C. Jesch, T. Dickel, W.R. Plaß, D. Short, S. Ayet San Andres, J. Dilling, H. Geissel, F. Greiner, J. Lang, K.G. Leach, W. Lippert, C. Scheidenberger, M.I. Yavor, The mr-tof-ms isobar separator for the titan facility at TRIUMF, Hyperfine Interact. 235 (1) (2015) 97–106.

[15] P. Chauveau, P. Delahaye, G. De France, S. El Abir, J. Lory, Y. Merrer, M. Rosenbusch, L. Schweikhard, R. Wolf, Pilgrim, a multi-reflection time-of-flight mass spectrometer for Spiral2-S3 at GANIL, in: Proceedings of the XVIIth International Conference on Electromagnetic Isotope Separators and Related Topics (EMIS2015), Grand Rapids, MI, U.S.A., 11–15 May 2015, Nucl. Instrum. Methods Phys. Res. B 376 (2016) 211–215.

[16] B. Liu, M. Brodeur, D. Burdette, J. Kelly, T. Kim, J. Long, P. O'Malley, The performance of the commissioned Notre Dame multi-reflection time-of-flight mass spectrometer, Nucl. Instrum. Methods Phys. Res. A 985 (2021) 164679.

[17] H. Wollnik, M. Przewloka, Time-of-flight mass spectrometers with multiply reflected ion trajectories, Int. J. Mass Spectrom. Ion Process. 96 (3) (1990) 267–274.

[18] D. Zajfman, O. Heber, L. Vejby-Christensen, I. Ben-Itzhak, M. Rappaport, R. Fishman, M. Dahan, Electrostatic bottle for long-time storage of fast ion beams, Phys. Rev. A 55 (1997) R1577–R1580.

[19] W.H. Benner, A gated electrostatic ion trap to repetitiously measure the charge and m/z of large electrospray ions, Anal. Chem. 69 (10) (1997) 4162–4168.

[20] F. Wienholtz, D. Atanasov, S. Kreim, V. Manea, M. Rosenbusch, L. Schweikhard, A. Welker, R.N. Wolf, Towards ultrahigh-resolution multi-reflection time-of-flight mass spectrometry at isoltrap, Phys. Scr. 2015 (11) (2015) 014068.

[21] T. Dickel, M.I. Yavor, J. Lang, W.R. Plaß, W. Lippert, H. Geissel, C. Scheidenberger, Dynamical time focus shift in multiple-reflection time-of-flight mass spectrometers, Int. J. Mass Spectrom. 412 (2017) 1–7.

[22] E. Leistenschneider, M.P. Reiter, S. Ayet San Andrés, B. Kootte, J.D. Holt, P. Navrátil, C. Babcock, C. Barbieri, B.R. Barquest, J. Bergmann, J. Bollig, T. Brunner, E. Dunling, A. Finlay, H. Geissel, L. Graham, F. Greiner, H. Hergert, C. Hornung, C. Jesch, R. Klawitter, Y. Lan, D. Lascar, K.G. Leach, W. Lippert, J.E. McKay, S.F. Paul, A. Schwenk, D. Short, J. Simonis, V. Somà, R. Steinbrügge, S.R. Stroberg, R. Thompson, M.E. Wieser, C. Will, M. Yavor, C. Andreoiu, T. Dickel, I. Dillmann, G. Gwinner, W.R. Plaß, C. Scheidenberger, A.A. Kwiatkowski, J. Dilling, Dawning of the N = 32 shell closure seen through precision mass measurements of neutron-rich titanium isotopes, Phys. Rev. Lett. 120 (2018) 062503.

[23] Y. Ito, P. Schury, M. Wada, F. Arai, H. Haba, Y. Hirayama, S. Ishizawa, D. Kaji, S. Kimura, H. Koura, M. MacCormick, H. Miyatake, J.Y. Moon, K. Morimoto, K. Morita, M. Mukai, I. Murray, T. Niwase, K. Okada, A. Ozawa, M. Rosenbusch, A. Takamine, T. Tanaka, Y.X. Watanabe, H. Wollnik, S. Yamaki, First direct mass measurements of nuclides around Z = 100 with a multireflection time-of-flight mass spectrograph, Phys. Rev. Lett. 120 (2018) 152501.

[24] S. Ayet San Andrés, C. Hornung, J. Ebert, W.R. Plaß, T. Dickel, H. Geissel, C. Scheidenberger, J. Bergmann, F. Greiner, E. Haettner, C. Jesch, W. Lippert, I. Mardor, I. Miskun, Z. Patyk, S. Pietri, A. Pihktelev, S. Purushothaman, M.P. Reiter, A.-K. Rink, H. Weick, M.I. Yavor, S. Bagchi, V. Charviakova, P. Constantin, M. Diwisch, A. Finlay, S. Kaur, R. Knöbel, J. Lang, B. Mei, I.D. Moore, J.-H. Otto, I. Pohjalainen, A. Prochazka, C. Rappold, M. Takechi, Y.K. Tanaka, J.S. Winfield, X. Xu, High-resolution, accurate multiple-reflection time-of-flight mass spectrometry for short-lived, exotic nuclei of a few events in their ground and low-lying isomeric states, Phys. Rev. C 99 (2019) 064313.

[25] R.F. Garcia Ruiz, R. Berger, J. Billowes, C.L. Binnersley, M.L. Bissell, A.A. Breier, A.J. Brinson, K. Chrysalidis, T.E. Cocolios, B.S. Cooper, K.T. Flanagan, T.F. Giesen, R.P. de Groote, S. Franchoo, F.P. Gustafsson, T.A. Isaev, Á. Koszorús, G. Neyens, H.A. Perrett, C.M. Ricketts, S. Rothe, L. Schweikhard, A.R. Vernon, K.D.A. Wendt, F. Wienholtz, S.G. Wilkins, X.F. Yang, Spectroscopy of short-lived radioactive molecules, Nature 581 (2020) 396.

[26] A. Gottberg, T. Mendonca, R. Luis, J. Ramos, C. Seiffert, S. Cimmino, S. Marzari, B. Crepieux, V. Manea, R. Wolf, F. Wienholtz, S. Kreim, V. Fedosseev, B. Marsh, S. Rothe, P. Vaz, J. Marques, T. Stora, Experimental tests of an advanced proton-to-neutron converter at ISOLDE-CERN, Nucl. Instrum. Methods Phys. Res. B 336 (2014) 143–148.

[27] K. Chrysalidis, J. Ballof, C.E. Düllmann, V.N. Fedosseev, C. Granados, B.A. Marsh, Y. Martinez Palenzuela, J.P. Ramos, S. Rothe, T. Stora, K. Wendt, Developments towards the delivery of selenium ion beams at ISOLDE, Eur. Phys. J. A 55 (10) (2019) 173.

[28] R.N. Wolf, D. Beck, K. Blaum, C. Böhm, C. Borgmann, M. Breitenfeldt, N. Chamel, S. Goriely, F. Herfurth, M. Kowalska, S. Kreim, D. Lunney, V. Manea, E. Minaya Ramirez, S. Naimi, D. Neidherr, M. Rosenbusch, L. Schweikhard, J. Stanja, F. Wienholtz, K. Zuber, Plumbing neutron stars to new depths with the binding energy of the exotic nuclide ^{82}Zn, Phys. Rev. Lett. 110 (2013) 041101.

[29] B.A. Marsh, T. Day Goodacre, S. Sels, Y. Tsunoda, B. Andel, A.N. Andreyev, N.A. Althubiti, D. Atanasov, A.E. Barzakh, J. Billowes, K. Blaum, T.E. Cocolios, J.G. Cubiss, J. Dobaczewski, G.J. Farooq-Smith, D.V. Fedorov, V.N. Fedosseev, K.T. Flanagan, L.P. Gaffney, L. Ghys, M. Huyse, S. Kreim, D. Lunney, K.M. Lynch, V. Manea, Y. Martinez Palenzuela, P.L. Molkanov, T. Otsuka, A. Pastore, M. Rosenbusch, R.E. Rossel, S. Rothe, L. Schweikhard, M.D. Seliverstov, P. Spagnoletti, C. Van Beveren, P. Van Duppen, M. Veinhard, E. Verstraelen, A. Welker, K. Wendt, F. Wienholtz, R.N. Wolf, A. Zadvornaya, K. Zuber, Characterization of the shape-staggering effect in mercury nuclei, Nat. Phys. 14 (2018) 1163.

[30] T. Day Goodacre, A.V. Afanasjev, A.E. Barzakh, B.A. Marsh, S. Sels, P. Ring, H. Nakada, A.N. Andreyev, P. Van Duppen, N.A. Althubiti, B. Andel, D. Atanasov, J. Billowes, K. Blaum, T.E. Cocolios, J.G. Cubiss, G.J. Farooq-Smith, D.V. Fedorov, V.N. Fedosseev, K.T. Flanagan, L.P. Gaffney, L. Ghys, M. Huyse, S. Kreim, D. Lunney, K.M. Lynch, V. Manea, Y. Martinez Palenzuela, P.L. Molkanov, M. Rosenbusch, R.E. Rossel, S. Rothe, L. Schweikhard, M.D. Seliverstov, P. Spagnoletti, C. Van Beveren, M. Veinhard, E. Verstraelen, A. Welker, K. Wendt, F. Wienholtz, R.N. Wolf, A. Zadvornaya, K. Zuber, Laser spectroscopy of neutron-rich ^{207,208}Hg isotopes: Illuminating the kink and odd-even staggering in charge radii across the N = 126 shell closure, Phys. Rev. Lett. 126 (2021) 032502.

[31] F.M. Maier, Laser Spectroscopy of Short-Lived- Radionuclides in an Ion Trap: MIRACLS' proof-of-principle experiment and the simulation of the future 30-keV MR-ToF device (M.Sc. thesis), Johannes Kepler University Linz, 2019.

[32] M. Rosenbusch, S. Kemnitz, R. Schneider, L. Schweikhard, R. Tschiersch, R.N. Wolf, Towards systematic investigations of space-charge phenomena in multi-reflection ion traps, AIP Conf. Proc. 1521 (1) (2013) 53–62.

[33] M. Rosenbusch, P. Chauveau, P. Delahaye, G. Marx, L. Schweikhard, F. Wienholtz, R.N. Wolf, Delayed bunching for multi-reflection time-of-flight mass separation, AIP Conf. Proc. 1668 (1) (2015) 050001.

[34] F.M. Maier, P. Fischer, H. Heylen, V. Lagaki, S. Lechner, P. Plattner, S. Sels, F. Wienholtz, W. Nörtershäuser, L. Schweikhard, S. Malbrunot-Ettenauer, Simulations of a proof-of-principle experiment for collinear laser spectroscopy within a multi-reflection time-of-flight device, Hyperfine Interact. 240 (1) (2019) 54.

[35] S. Lechner, P. Fischer, H. Heylen, V. Lagaki, F. Maier, P. Plattner, M. Rosenbusch, S. Sels, F. Wienholtz, R.N. Wolf, W. Nörtershäuser, L. Schweikhard, S. Malbrunot-Ettenauer, Fluorescence detection as a new diagnostics tool for electrostatic ion beam traps, Hyperfine Interact. 240 (1) (2019) 95.

[36] V. Lagaki, P. Fischer, H. Heylen, F. Hummer, S. Lechner, S. Sels, F. Maier, P. Plattner, M. Rosenbusch, F. Wienholtz, R. Wolf, W. Nörtershäuser, L. Schweikhard, S. Malbrunot-Ettenauer, Stray-light suppression for the MIRACLS proof-of-principle experiment, Acta Phys. Polon. B 51 (2020) 571–576.

[37] S. Sels, P. Fischer, H. Heylen, V. Lagaki, S. Lechner, F. Maier, P. Plattner, M. Rosenbusch, F. Wienholtz, R. Wolf, W. Nörtershäuser, L. Schweikhard, S. Malbrunot-Ettenauer, First steps in the development of the multi ion reflection apparatus for collinear laser spectroscopy, Nucl. Instrum. Methods Phys. Res. B 463 (2020) 310–314.

[38] T. Murböck, S. Schmidt, Z. Andelkovic, G. Birkl, W. Nörtershäuser, M. Vogel, A compact source for bunches of singly charged atomic ions, Rev. Sci. Instrum. 87 (4) (2016) 043302.

[39] K. Kreim, M. Bissell, J. Papuga, K. Blaum, M.D. Rydt, R.G. Ruiz, S. Goriely, H. Heylen, M. Kowalska, R. Neugart, G. Neyens, W. Nörtershäuser, M. Rajabali, R.S. Alarcón, H. Stroke, D. Yordanov, Nuclear charge radii of potassium isotopes beyond N=28, Phys. Lett. B 731 (2014) 97–102.

[40] W. Gins, R.P. de Groote, M.L. Bissell, C. Granados Buitrago, R. Ferrer, K.M. Lynch, G. Neyens, S. Sels, Analysis of counting data: Development of the satlas python package, Comput. Phys. Comm. 222 (2018) 286–294.

[41] R.T. Birge, The calculation of errors by the method of least squares, Phys. Rev. 40 (1932) 207–227.

[42] P.D. Group, P.A. Zyla, R.M. Barnett, J. Beringer, O. Dahl, D.A. Dwyer, D.E. Groom, C.J. Lin, K.S. Lugovsky, E. Pianori, D.J. Robinson, C.G. Wohl, W.M. Yao, K. Agashe, G. Aielli, B.C. Allanach, C. Amsler, M. Antonelli, E.C. Aschenauer, D.M. Asner, H. Baer, S. Banerjee, L. Baudis, C.W. Bauer, J.J. Beatty, V.I. Belousov, S. Bethke, A. Bettini, O. Biebel, K.M. Black, E. Blucher, O. Buchmuller, V. Burkert, M.A. Bychkov, R.N. Cahn, M. Carena, A. Ceccucci, A. Cerri, D. Chakraborty, R.S. Chivukula, G. Cowan, G. D'Ambrosio, T. Damour, D. de Florian, A. de Gouvêa, T. DeGrand, P. de Jong, G. Dissertori, B.A. Dobrescu, M. D'Onofrio, M. Doser, M. Drees, H.K. Dreiner, P. Eerola, U. Egede, S. Eidelman, J. Ellis, J. Erler, V.V. Ezhela, W. Fetscher, B.D. Fields, B. Foster, A. Freitas, H. Gallagher, L. Garren, H.J. Gerber, G. Gerbier, T. Gershon, Y. Gershtein, T. Gherghetta, A.A. Godizov, M.C. Gonzalez-Garcia, M. Goodman, C. Grab, A.V. Gritsan, C. Grojean, M. Grünewald, A. Gurtu, T. Gutsche, H.E. Haber, C. Hanhart, S. Hashimoto, Y. Hayato, A. Hebecker, S. Heinemeyer, B. Heltsley, J.J. Hernández-Rey, K. Hikasa, J. Hisano, A. Höcker, J. Holder, A. Holtkamp, J. Huston, T. Hyodo, K.F. Johnson, M. Kado, M. Karliner, U.F. Katz, M. Kenzie, V.A. Khoze, S.R. Klein, E. Klempt, R.V. Kowalewski, F. Krauss, M. Kreps, B. Krusche, Y. Kwon, O. Lahav, J. Laiho, L.P. Lellouch, J. Lesgourgues, A.R. Liddle, Z. Ligeti, C. Lippmann, T.M. Liss, L. Littenberg, C. Lourengo, S.B. Lugovsky, A. Lusiani, Y. Makida, F. Maltoni, T. Mannel, A.V. Manohar, W.J. Marciano, A. Masoni, J. Matthews, U.G. Meißner, M. Mikhasenko, D.J. Miller, D. Milstead, R.E. Mitchell, K. Mönig, P. Molaro, F. Moortgat, M. Moskovic, K. Nakamura, M. Narain, P. Nason, S. Navas, M. Neubert, P. Nevski, Y. Nir, K.A. Olive, C. Patrignani, J.A. Peacock, S.T. Petcov, V.A. Petrov, A. Pich, A. Piepke, A. Pomarol, S. Profumo, A. Quadt, K. Rabbertz, J. Rademacker, G. Raffelt, H. Ramani, M. Ramsey-Musolf, B.N. Ratcliff, P. Richardson, A. Ringwald, S. Roesler, S. Rolli, A. Romaniouk, L.J. Rosenberg, J.L. Rosner, G. Rybka, M. Ryskin, R.A. Ryutin, Y. Sakai, G.P. Salam, S. Sarkar, F. Sauli, O. Schneider, K. Scholberg, A.J. Schwartz, J. Schwiening, D. Scott, V. Sharma, S.R. Sharpe, T. Shutt, M. Silari, T. Sjöstrand, P. Skands, T. Skwarnicki, G.F. Smoot, A. Soffer, M.S. Sozzi, S. Spanier, C. Spiering, A. Stahl, S.L. Stone, Y. Sumino, T. Sumiyoshi, M.J. Syphers, F. Takahashi, M. Tanabashi, J. Tanaka, M. Taševský, K. Terashi, J. Terning, U. Thoma, R.S. Thorne, L. Tiator, M. Titov, N.P. Tkachenko, D.R. Tovey, K. Trabelsi, P. Urquijo, G. Valencia, R. Van de Water, N. Varelas, G. Venanzoni, L. Verde, M.G. Vincter, P. Vogel, W. Vogelsang, A. Vogt, V. Vorobyev, S.P. Wakely, W. Walkowiak, C.W. Walter, D. Wands, M.O. Wascko, D.H. Weinberg, E.J. Weinberg, M. White, L.R. Wiencke, S. Willocq, C.L. Woody, R.L. Workman, M. Yokoyama, R. Yoshida, G. Zanderighi, G.P. Zeller, O.V. Zenin, R.Y. Zhu, S.L. Zhu, F. Zimmermann, J. Anderson, T. Basaglia, V.S. Lugovsky, P. Schaffner, W. Zheng, Review of particle physics, Prog. Theor. Exp. Phys. 2020 (08) (2020) 083C01.

[43] V. Batteiger, S. Knünz, M. Herrmann, G. Saathoff, H.A. Schüssler, B. Bernhardt, T. Wilken, R. Holzwarth, T.W. Hänsch, T. Udem, Precision spectroscopy of the $3s$–$3p$ fine-structure doublet in Mg^+, Phys. Rev. A 80 (2009) 022503.

[44] L. Fischer, Improvements of the Mg Ion Beam Intensity for the Proof-of-Principle Experiment of Collinear Laser Spectroscopy on Short-Lived Nuclides in a Multi Ion Reflection Apparatus (B.Sc. thesis), Karlsruhe Institute of Technology, 2018.

[45] F. Hummer, Investigation of Space Charge Effects in MIRACLS' Proof-of- Principle MR-ToF Device (B.Sc. thesis), Johannes Kepler University Linz, 2019.

[46] H. Frånberg, P. Delahaye, J. Billowes, K. Blaum, R. Catherall, F. Duval, O. Gianfrancesco, T. Giles, A. Jokinen, M. Lindroos, D. Lunney, E. Mane, I. Podadera, Off-line commissioning of the ISOLDE cooler, in: Proceedings of the XVth International Conference on Electromagnetic Isotope Separators and Techniques Related To their Applications, Nucl. Instrum. Methods Phys. Res. B 266 (19) (2008) 4502–4504.

[47] E. Mané, J. Billowes, K. Blaum, P. Campbell, B. Cheal, P. Delahaye, K.T. Flanagan, D.H. Forest, H. Franberg, C. Geppert, T. Giles, A. Jokinen, M. Kowalska, R. Neugart, G. Neyens, W. Nörtershäuser, I. Podadera, G. Tungate, P. Vingerhoets, D.T. Yordanov, An ion cooler-buncher for high-sensitivity collinear laser spectroscopy at ISOLDE, Eur. Phys. J. A 42 (3) (2009) 503–507.

[48] A. Koszorús, X.F. Yang, J. Billowes, C.L. Binnersley, M.L. Bissell, T.E. Cocolios, G.J. Farooq-Smith, R.P. de Groote, K.T. Flanagan, S. Franchoo, R.F. Garcia Ruiz, S. Geldhof, W. Gins, A. Kanellakopoulos, K.M. Lynch, G. Neyens, H.H. Stroke, A.R. Vernon, K.D.A. Wendt, S.G. Wilkins, Precision measurements of the charge radii of potassium isotopes, Phys. Rev. C 100 (2019) 034304.

[49] Á. Koszorús, X.F. Yang, W.G. Jiang, S.J. Novario, S.W. Bai, J. Billowes, C.L. Binnersley, M.L. Bissell, T.E. Cocolios, B.S. Cooper, R.P. de Groote, A. Ekström, K.T. Flanagan, C. Forssén, S. Franchoo, R.F.G. Ruiz, F.P. Gustafsson, G. Hagen, G.R. Jansen, A. Kanellakopoulos, M. Kortelainen, W. Nazarewicz, G. Neyens, T. Papenbrock, P.G. Reinhard, C.M. Ricketts, B.K. Sahoo, A.R. Vernon, S.G. Wilkins, Charge radii of exotic potassium isotopes challenge nuclear theory and the magic character of n = 32, Nat. Phys. 17 (2021) 439.

[50] M. Verlinde, K. Dockx, S. Geldhof, K. König, D. Studer, T.E. Cocolios, R.P. de Groote, R. Ferrer, Y. Kudryavtsev, T. Kieck, I. Moore, W. Nörtershäuser, S. Raeder, P. Van den Bergh, P. Van Duppen, K. Wendt, On the performance of wavelength meters: Part 1—consequences for medium-to-high-resolution laser spectroscopy, Appl. Phys. B 126 (5) (2020) 85.

[51] K. König, P. Imgram, J. Krämer, B. Maaß, K. Mohr, T. Ratajczyk, F. Sommer, W. Nörtershäuser, On the performance of wavelength meters: Part 2—frequency-comb based characterization for more accurate absolute wavelength determinations, Appl. Phys. B 126 (5) (2020) 86.